RSC Advances

ROYAL SOCIETY OF CHEMISTRY

www.rsc.org/advances

The instability of S vacancy in Cu_2ZnSnS_4

Xiaoli Zhang[1], Miaomiao Han[1], Zhi Zeng[1,2*], and Hai Qing Lin[3]

[1]*Key Laboratory of Materials Physics, Institute of Solid State Physics, CAS,*

[2]*Department of Physics, University of Science and Technology of China, Hefei 230031, China*

[3]*Beijing Computational Science Research Center, Beijing 100084, China*

(Dated: January 22, 2016)

Abstract

The electronic structures of the possible charge states of vacancies in the earth-abundant solar cell absorber material Cu_2ZnSnS_4 (CZTS) are investigated using the screened-exchange hybrid density functional theory. We find out that all the charge states of anion S vacancy (V_S) are not stable because V_S rehybridizes with the nearest neighbor Sn atom reducing the valence of the Sn atom. Therefore, there is no charge transition level for V_S. Instead, all the charge states of cation vacancies are stable. The copper and zinc vacancies show delocalized feature which create shallow charge transition levels, while the tin vacancy shows localized feature which creates deep charge transition levels within the band gap and acts as recombination center in CZTS.

PACS numbers:

* Correspondence author: zzeng@theory.issp.ac.cn

Introduction

$Cu(In,Ga)Se_2$ (CIGS) possesses the highest energy conversion efficiency up to 21.7% among the thin film solar cells.[1] Researchers are still making their efforts on improving the CIGS solar cell efficiency. CIGS solar cells compete today as successors of the dominating silicon technology. Nevertheless, there are concerns about their large scale production due to the price and the availability of In. By replacing In and Ga elements in CIGS with Zn and Sn elements it formulates $Cu_2ZnSnSe_4$ (CZTSe),[2] which is very similar to Cu_2ZnSnS_4 (CZTS) in structure and physical properties.[3, 4] CZTS and CZTSe quaternary compounds overcome the disadvantages in CIGS owing to their earth-abundant and low-toxicity constituents. Moreover, the kesterite CZTS possesses the $I\bar{4}$ space group,[5] typical optimal band gap of about 1.5 eV[6, 7] (band gap of CZTSe is 1.0 eV) and large absorption coefficient of more than 10^4 cm^{-1}.[8] The energy conversion efficiency of CZTS-based solar cell keeps a world record of 12.6%.[9] The relatively high energy conversion efficiency is partly due to the *p*-type conductivity via inducing the intrinsic point defects in the parent CZTS. Point defects significantly influence the efficiency of the *pn*-junction-based solar cells. Therefore, much attention has been paid to the point defects in CZTS to understand the relationship between defects and solar cell efficiency.[10–15]

The charge transition levels within the band gap determine the solar cell performances, which are obtained from first-principles calculations and can be directly compared with the experimental activation energies. Deep defect levels may act as recombination centers, while shallow defect levels allow the transformation from one charge state to another easily which will increase carrier concentration in solar cell devices. The charge transition levels for defects in CZTS have been studied extensively.[12, 13, 15] For the vacancies in CZTS, copper vacancy (V_{Cu}) was found to have a very shallow acceptor level above the valence band while tin vacancy (V_{Sn}) have deep levels within the band gap.[12, 13, 15] The levels of zinc vacancy (V_{Zn}) lie in between that of V_{Cu} and V_{Sn}.[12, 13, 15] But for sulfur vacancy (V_S), different groups gave different results. Chen *et al.*[13] showed that V_S produced a deep $\epsilon(0/2+)$ level within the band gap, while Han *et al.*[15] claimed no charge transition level within the band gap. To understand the reason of this discrepancy, we list the expression of the charge transition level:

$$\epsilon(q/q') = (E(\alpha, q) - E(\alpha, q'))/(q' - q) \quad (1)$$

where $E(\alpha, q)$ and $E(\alpha, q')$ denote the total energies of a defect with charge states q and q', respectively. From the Eq.(1) we can see the theoretical value of a defect charge transition level is related to the total energy difference of the involved two different charge states of the defect, which was always taken in previous studies.[12–15] However, the way of inspecting total energy difference ignores examining the stability of the considered charge states, which may lead to theoretically unphysical defect transition levels[18–21]. This might be the reason why consensus have not made for the charge transition level of V_S. Therefore, in this paper, we are motivated to examine the stability of the possible charge states of vacancies in CZTS.

The stability of a charge states can be justified by using band structures and defect-induced single particle levels (Kohn-Sham eigenvalues) analysis, which has been applied on other semiconductors.[18–21] A defect often has multiple possible charge states. The stability of these possible charge states is strongly related to the positions of the defect-induced single particle levels relative to the band gap. To pick out the defect-induced single levels, we examine the local density of states (LDOS) of vacancy systems which corresponds to the DOS of the nearest neighbor atoms around the vacant site. The additional sharp peaks in LDOS of a vacancy system compared with that of parent compound are defect-induced single particle levels. If the defect-induced single particle levels lie within the band gap, the corresponding charge state is stable because the defect-induced single particle levels may form a stable bound state bounding electrons or holes. If the defect-induced single particle levels stay in the VB or conduction band (CB), the corresponding charge state is unstable because the defect-induced single particle levels are always occupied or unoccupied so that the electrons or holes on them are communized. We should keep in mind that defect-induced single particle level analysis here is a qualitative view of the defects in CZTS, which helps us to obtain physically meaningful charge transition levels. With the knowledge of the stable charge states of a defect provided by the present work, we could further calculate the charge transition levels by Eq. (1) just as other DFT calculations.[12–15]

In this paper, using the screened-exchange hybrid density functional theory we study the electronic structure of all the possible charge states of vacancies in CZTS. Our results show that all the charge states of V_S are not stable, resulting that V_S creates none charge transition level within the band gap. This is caused by the rehybridization of V_S with the nearest neighbor Sn atom, which reduces the valence of the Sn atom. Instead, all the charge states of cation vacancies are stable, which can create either shallow (V_{Cu} and V_{Zn}) or deep

(V_{Sn}) charge transition levels depending on their delocalization or localization properties. Therefore, the performance of CZTS solar cells could be improved from the cation vacancy engineering due to that the charge transition energy levels can arise from the cation vacancies but rather anion vacancy.

Computational details

The electronic structure calculations are carried out using the density functional theory as implemented in the plane wave VASP code[22]. For the exchange-correlation functional, both generalized gradient approximation (GGA) of Perdew-Burke-Ernzerhof (PBE)[23, 24] and screened Coulomb hybrid functional Heyd-Scuseria-Ernzerhof (HSE06) are used [25, 26]. PBE-GGA is used to obtain an initial structures and HSE06 is used to calculate the electronic structures, since GGA often under estimates the band gap of Cu-based semiconductors and HSE06 functional describes the localized Cu $3d$ orbitals more correctly than (semi)local-density functionals[27] by separating the electron-electron interaction into a short- and long-ranged part and substituting part of short range PBE-GGA exchange energy with the short range Hartree-Fock (HF) exchange energy. HSE06 functional has been verified to improve the description of the band gap of CZTS as well as the defect properties.[13, 15] The parameter controlling the amount of HF exchange in the HSE06 functional is set to 0.3 and the range-separation screening parameter μ is set to 0.20 $Å^{-1}$. The interaction between ions and electrons is described by the projector-augmented wave (PAW) method.[28, 29] The cutoff energy for the plane-wave basis is set to 300 eV. Using these setup our calculated band gap of 1.43 eV is close to the reported 1.44 $\sim$ 1.51 eV for CZTS.[6, 7] The vacancy models are constructed by removing an atom from a 64-atom 2×2×1 supercell. The Brillouin zone sampling is done using 2×2×2 k-point mesh. The ground state geometries of all the defect systems are obtained by minimizing the Hellman-Feynman forces on each atom to become less than 0.05 eV/Å. We also perform 432-atom 3×3×3 supercells in this paper, for which PBE-GGA is used for both structure optimizations and electronic structure investigations. And Γ only k-point mesh in the Brillouin zone is used.

Results and discussions

In Cu-based compound semiconductors, cation vacancies and anion vacancies are acceptors and donors, respectively. Therefore, in general, V_{Cu} could posses 0 and 1- two charge states, V_{Zn} could posses 0, 1- and 2- three charge states, V_{Sn} could posses 0, 1-, 2-, 3- and 4- five charge states, and V_S could posses 0, 1+ and 2+ three charge states in CZTS. Considering that the Cu(I) can be oxidized into Cu(II) in the kesterite material, we also investigate the 2- charge state of V_{Cu}. Various charge states have different impact on the crystal structures as well as the electronic structures. Therefore, in this paper, the crystal structures respect to all the charge states of vacancies are fully optimized, where Fig.1 illustrates the selective optimized structures. In CZTS, each cation is tetrahedrally surrounded by four S atoms, while each anion S atom is surrounded by two Cu, one Zn and one Sn atoms. Largest distortions happen at atoms around the vacant site, so that only the four nearest neighbor atoms around the vacant site are shown in Fig. 1.

We first discuss the crystal distortions of cation vacancies. After removing a Cu atom, the four nearest neighbor S atoms move toward the vacant site, resulting that the V_{Cu}-S bond lengths decrease about 0.02 Å compared with the parent compound. V_{Cu} is an accepter which could capture one and two electrons forming V_{Cu}^{1-} and V_{Cu}^{2-} charge states, respectively. The four nearest neighbor S atoms move backward the vacant site leading to that V_{Cu}-S bond lengths increase about 0.02 Å and 0.06 Å for V_{Cu}^{1-} and V_{Cu}^{2-}, respectively, compared with that of the parent compound. The displacements of four S atoms around the vacant site for V_{Cu}^{1-} are shown in Fig. 1(a). The opposite displacements of four S atoms around the vacant site in V_{Cu}^{0} and V_{Cu}^{1-} are caused by the competition of strain induced by the vacancy and electrostatic repulsion between the four S atoms. For V_{Cu}^{0}, the V_{Cu}-S bond lengths decrease to gain the strain energy. And for V_{Cu}^{1-}, the additional electron leads to the increasing of charge density on the four S atoms around the vacant site which increases the electrostatic repulsion. As a result, the bond lengths of V_{Cu}-S increase to gain the electrostatic repulsion in 1- and 2- charge states.

The neutral V_{Zn}^{0} can capture one and two electrons forming V_{Zn}^{1-} and V_{Zn}^{2-} charge states, respectively. The V_{Zn}-S bond lengths decrease about 0.06 Å and 0.04 Å for V_{Zn}^{0} and V_{Zn}^{1-}, respectively, while increase about 0.02 Å for V_{Zn}^{2-} as shown in Fig. 1(b). The different crystal displacements are also caused by the competition results of strain induced by the vacancy

and electrostatic repulsion between the four S atoms.

V_{Sn} can capture at most 4 electrons forming five charge states V_{Sn}^{0}, V_{Sn}^{1-}, V_{Sn}^{2-}, V_{Sn}^{3-} and V_{Sn}^{4-} . The variation of the V_{Sn}-S bond lengths are -0.09, -0.08, -0.04, 0.04 and 0.07 Å for V_{Sn}^{0}, V_{Sn}^{1-}, V_{Sn}^{2-}, V_{Sn}^{3-} and V_{Sn}^{4-}, respectively, as shown in Fig. 1(d-h). The structure changes are also the competition results of strain induced by the vacancy and electrostatic repulsion between the four S atoms around the vacant site. On one hand, the strength of the strain induced by a vacancy depends on the size mismatch. Among the three kind of cations in CZTS, Sn atom possesses the largest size mismatch, so that the displacement of four S atoms around the vacant site for neutral V_{Sn}^{0} is much larger than that of V_{Cu}^{0} and V_{Zn}^{0}. On the other hand, the strengths of the electrostatic repulsion between the four S atoms around the vacant site increase with the increasing charge state of the defect. As a result, the more electronegativity the longer the vacancy-S bond length for V_{Sn}.

To see the electronic structures of all the charge states of vacancies clearly, we plot their LDOS, as shown in Fig. 2. The Fig. 2(a) shows the LDOS of three charge states of V_{Cu}. V_{Cu}^{0} produces a hole in the valence band so that there are states cross the Fermi level forming a small peak at the Fermi level. With an additional electron forming V_{Cu}^{1-}, the electron and the hole compensates each other so that the valence band is fully occupied. The small peak move downward and located at about 0.25 eV below the Fermi level for V_{Cu}^{1-}. For V_{Cu}^{2-}, there is an additional electron compared with V_{Cu}^{1-} so that the electron occupies the conduction band. This can be seen from the LDOS of V_{Cu}^{2-}, the states of the valence band down shift of about 1.5 eV and there is also a small peak at the Fermi level. The Fig. 2(b) shows the LDOS of V_{Zn}^{0}, V_{Zn}^{1-} and V_{Zn}^{2-}. For V_{Zn}^{0}, there are two holes in the valence band, which cause two small peaks around the Fermi level with one at 0.2 eV above the Fermi level and one at 0.1 eV below the Fermi level. With an additional electron forming V_{Zn}^{1-}, there is one hole left in the valence band, which lead to the height of the peak above the Fermi level decreases compared with that of V_{Zn}^{0}. For V_{Zn}^{2-}, the two additional electrons compensate the two holes resulting a fully occupied valence band, so that the peak above the Fermi level disappears. The Fig. 2(c) shows the LDOS of five charge states of V_{Sn}. For V_{Sn}^{0}, there are four holes in the valence band, which cause two peaks around the Fermi level with one at 0.2 eV above the Fermi level and one at 0.1 eV below the Fermi level. With an additional electron forming V_{Sn}^{1-}, there are three holes left in the valence band, which lead to the heights of the peaks decrease compared with that of V_{Sn}^{0}. For V_{Sn}^{2-}, there are two holes left in the valence band,

which lead to the height of the peak above the Fermi level decreases and the height of the peak below the Fermi level greatly increases. For V_{Sn}^{3-}, there is one hole left in the valence band and the two peaks merged into one sharp peak at 0.1 eV below the Fermi level. For V_{Sn}^{4-}, the valence band is fully occupied with one sharp peak locates at 0.2 eV below the Fermi level. Comparing the heights of the peaks of all the charge states of cation vacancies discussed above, we find out that the peak heights of V_{Cu}^{0}, V_{Cu}^{1-} and V_{Cu}^{2-} are less than 2 and that for V_{Zn}^{0}, V_{Zn}^{1-}, V_{Zn}^{2-} as well as V_{Sn}^{0} and V_{Sn}^{1-} are less than 4 but that of V_{Sn}^{2-}, V_{Sn}^{3-} and V_{Sn}^{4-} are larger than 6. Therefore, we deduce that the V_{Sn}^{2-}, V_{Sn}^{3-} and V_{Sn}^{4-} show obvious localization feature, while V_{Sn}^{0} and V_{Sn}^{1-} as well as all the charge states of V_{Cu} and V_{Zn} show less obvious localization feature.

The localization feature of vacancies can also be seen from the defect-induced single particle levels within the band gap of the band structures, as shown in Fig. 3. For V_{Cu} and V_{Zn}, we only show the V_{Cu}^{1-} and V_{Zn}^{2-} which correspond to the highest LDOS peaks among all the charge states of V_{Cu} and V_{Zn}, respectively (see Fig. 3). For V_{Cu}^{1-}, the defect-induced single particle levels do not change the valence band top much compared with the parent material, which indicates very delocalized feature of V_{Cu}. For V_{Zn}^{2-}, the two top most valence bands are slightly lifted up along the Z-Γ and Γ-X lines. Thus the defect-induced single particle levels are less dispersion compared to the case of V_{Cu}^{1-}, implying the less delocalized feature of V_{Zn}^{2-} than V_{Cu}^{1-}. This is in accordance with the results of the LDOS in Fig. 2, in which the peaks of V_{Zn}^{2-} are higher than that of V_{Cu}^{1-}. For V_{Sn}, the large crystal distortions lift three top most valence bands up. The band widths of the three top most bands decrease with the increasing electronegativity. The defect-induced localized single particle levels of V_{Sn}^{2-}, V_{Sn}^{3-} and V_{Sn}^{4-} are marked with red dashed lines as shown in Fig. 3, where the localized feature can be clearly seen from the much more flat valance band top compared with the parent compound. Unlike higher charge states, the two topmost single particle levels do not show obvious localized characteristic in the lower V_{Sn}^{1-} and V_{Sn}^{0} charge states according to LDOS results.

The above electronic structure analysis shows that the V_{Sn}^{2-}, V_{Sn}^{3-} and V_{Sn}^{4-} exhibit obvious localized feature, but V_{Sn}^{0} and V_{Sn}^{1-} and all the charge states of V_{Zn} and V_{Cu} do not in 64-atom supercells. One possible reason is the finite-size effect, i.e., the defect and image interaction increases the band dispersion of defect system because of the small supercell and periodic boundary condition we are taken. As a result, the states of the delocalized defects

are hard to be separated from the valence band. The finite-size effect of defects was ever discussed in the $CuInSe_2$ and $CuGaSe_2$ by Pohl *et al.* where they found that most defects shew localized single-particle levels within the band gap when supercells larger than 216-atom were used.[20] For further clarification, here we use a 432-atom supercell with PBE calculations to check the finite-size effect of the vacancies in CZTS. The 432-atom supercell LDOS for V_{Cu}^{1-}, V_{Zn}^{2-}, V_{Sn}^{0} and V_{Sn}^{1-} are shown in Fig. 4. From the LDOS we can clearly see that the height of the peaks around the Fermi level of V_{Cu}^{1-} are smaller than 2, suggesting strong delocalized feature. The delocalized character of V_{Cu} is very similar to that of V_{Cu} in $CuInSe_2$ and $CuGaSe_2$, in which V_{Cu} is a shallow acceptor.[19, 20] The delocalization feature of V_{Cu} in CZTS implies that V_{Cu} is also a shallow level accepter, which is in accordance with other experimental and theoretical evidences.[13, 15] Therefore, V_{Cu} might be a hydrogenic effective-mass-like defect. The peak heights of V_{Sn}^{0} and V_{Sn}^{1-} increase to a value larger than 6, which demonstrate V_{Sn}^{0} and V_{Sn}^{1-} are localized defect. The localized defects often create deep defect levels because electrons on them are strongly bonded to the defect and hard to be ionized. This implies that the charge transition levels of V_{Sn} are deep in the band gap, in accordance with the calculated charge transition level by Chen *et al.*[13] For, V_{Zn}^{2-} the heights of the peaks around Fermi level are larger than that of V_{Cu}^{1-} but smaller than that of V_{Sn}^{0} and V_{Sn}^{1-} (see Fig. 4), which indicate that the localization feature of V_{Zn}^{2-} lies in between that of the V_{Cu}^{1-} and V_{Sn}^{1-}. As a result, the charge transition levels of V_{Zn} also lie in between that of V_{Cu} and V_{Zn}. Therefore, V_{Sn} main act as recombination center which need to be avoided in the high efficiency solar cell performances, while V_{Cu} is a shallow acceptor which need to be promoted to improve the solar cell efficiency.

Different from cation vacancies which are surrounded by four S atoms, S vacany is surrounded by one Sn, one Zn and two Cu atoms. In V_S^0, the Sn atom moves toward the vacant site with the V_S-Sn bond length decreasing about 0.53 Å. But the Zn and Cu atoms move backward the vacant site with the V_S-Zn and V_S-Cu bond lengths increasing about 0.36 Å and 0.54 Å, respectively (see Fig. 1(c)). The opposite displacement of Sn compared with Cu and Zn atoms indicates that larger amount of electrons transferred to Sn than Cu and Zn atoms. We calculated the Bader charge using Baders quantum theory of atoms in molecules (QTAIM) method[30] for the four atoms around the vacant site in the 64-atom supercell containing a S vacancy, which shows that the number of electrons on Sn atom increase about 0.49, while the number of electrons on the nearest Cu and Zn atoms increase 0.04 and

0.05, respectively, for V_S^0 compared with the parent material as shown in Table I. The LDOS in Fig. 2(d) shows that states around Fermi level for V_S^0 are less than 1. The situations of V_S^{1+} and V_S^{2+} are similar to that of V_S^0. This indicates that the transferred electrons on Sn atom from the defect are not localized defect electrons. Therefore, we conclude that the transferred electrons on Sn atom mainly decrease the valence of the Sn atom because Sn atom has multiple valence states, which has the ability to capture additional electrons to decrease its valence. In addition, if the electrons transferred from the vacancy localized on Sn atom for V_S^0, V_S^0 could donate two electrons forming V_S^{2+}. Then the donated electrons might be mainly contributed by the Sn atom. However, for V_S^{2+}, the calculated Bader charge shows that the Cu, Zn and Sn atoms donated more or less the same amount of electrons (Cu(0.02), Zn(0.01) and Sn(0.03) see Table I) as well as other atoms in the supercell. This again implies that V_S rehybridized with Sn atom and decreases the valence of Sn. As a result, the various charge states of V_S are not stable, which also implies that V_S creates no charge transition level within the band gap. This is in consistent with the results by Han *et al.*,[15] where they found no defect transition level for V_S in the band gap.

Conclusion

In this work, we investigated the stability of all the possible charge states of the four vacancy defects in Cu_2ZnSnS_4 (CZTS) by employing screened Coulomb hybrid functional Heyd-Scuseria-Ernzerhof (HSE06). We find out that all the charge states of V_S are not stable because V_S rehybridizes with the nearest neighbor Sn atom, which reduces the valence of the Sn atom. Therefore, V_S creates no charge transition level within the band gap. All the charge states of cation vacancies are stable. V_{Cu} and V_{Zn} show delocalized feature while V_{Sn} show localized feature. The electronic structures of the cations implying that the V_{Cu} is a shallow level acceptor while V_{Sn} is a deep level acceptor. Therefore, V_{Sn} main act as recombination center which need to be avoided in the high efficiency solar cell performances, while the V_{Cu} shallow acceptor need to be promoted to improve the solar cell efficiency.

Acknowledgments

This work was supported by the special Funds for Major State Basic Research Project of China (973) under Grant No. 2012CB933702, the NSFC under Grant Nos. 11204310 and U1230202(NSAF). The calculations were performed in Center for Computational Science of CASHIPS and on the ScGrid of Supercomputing Center, Computer Network Information Center of CAS.

References

[1] Jackson, P. *et al.* Properties of Cu(In,Ga)Se_2 Solar Cells with New Record Efficiencies up to 21.7%. *Phys. Status Solidi RRL* **9**, 1, 28-31 (2015).

[2] Chen, S., Gong, X. G., Walsh, A. & Wei, S.-H. Electronic structure and stability of quaternary chalcogenide semiconductors derived from cation cross-substitution of II-VI and I-III-VI_2 compounds. *Phys. Rev. B* **79**, 165211 (2009).

[3] Chen, S., Gong, X. G., Walsh, A. & Wei, S.-H. Crystal and electronic band structure of Cu_2ZnSnX_4 (X = S and Se) photovoltaic absorbers: First-principles insights. *Appl. Phys. Lett.* **94**, 041903 (2009).

[4] Persson, C. Electronic and optical properties of Cu_2ZnSnS_4 and $Cu_2ZnSnSe_4$. *J. Appl. Phys.* **107**, 053710 (2010).

[5] Hall, S. R., Szymański, J. T. & Stewart, J. M. Kesterite, Cu_2(Zn, Fe)SnS_4, and stannite, Cu_2(Fe, Zn)SnS_4, structurally similar but distinct minerals. *Can. Mineral.* **16**, 131-137 (1978).

[6] Seol, J. S., Lee, S. Y., Lee, J. C., Nam, H. D. & Kim, K. H. Electrical and optical properties of Cu_2ZnSnS_4 thin films prepared by RF magnetron sputtering process. *Sol. Energy Mater. Sol. Cells* **75**, 155-162 (2003).

[7] Scragg, J. J., Dale, P. J. & Peter, L. M. Towards sustainable materials for solar energy conversion: Preparation and photoelectrochemical characterization of Cu_2ZnSnS_4. E*lectrochem. Comm.* **10**, 639 (2008).

[8] Ito, K. & Nakazawa, T. Electrical and optical properties of stannite-type quaternary semicon-

ductor thin films. *Jpn. J. Appl. Phys.* **27**, 11, 2094-2097 (1988).

[9] W. Wang *et al.* Device characteristics of CZTSSe thin-film solar cells with 12.6% efficiency. *Adv. Energy Mater.* **4**, 1301465 (2014).

[10] Zillner, E. *et al.* Lattice positions of Sn in Cu_2ZnSnS_4 nanoparticles and thin films studied by synchrotron X-ray absorption near edge structure analysis. *Appl. Phys. Lett.* **102**, 221908 (2013).

[11] Washio, T., Nozaki, H., Fukano, T., Motohiro, T., Jimbo, K. & Katagiri, H. Analysis of lattice site occupancy in kesterite structure of Cu_2ZnSnS_4 films using synchrotron radiation x-ray diffraction. *J. Appl. Phys.* **110**, 074511 (2011).

[12] Walsh, A., Chen, S., Wei, S.-H. & Gong, X. G. Kesterite thin-film solar cells: advances in materials modelling of Cu_2ZnSnS_4. *Adv. Energy Mater.* (2012).

[13] Chen, S., Walsh, A., Gong, X. G. & Wei, S.-H. Classification of lattice defects in the kesterite Cu_2ZnSnS_4 and $Cu_2ZnSnSe_4$ earth-abundant solar cell absorbers. *Adv. Mater.* **25**, 1522 (2013).

[14] Nagoya, A., Asahi, R., Wahl, R. & Kresse, G. Defect formation and phase stability of Cu_2ZnSnS_4 photovoltaic material. *Phys. Rev. B* **81**, 113202 (2010).

[15] Han, D. *et al.* Deep electron traps and origin of p-type conductivity in the earth-abundant solar-cell material Cu_2ZnSnS_4. *Phys. Rev. B* **87**, 155206 (2013).

[16] Hohenberg, P. & Kohn, W. Inhomogeneous electron gas. *Phys. Rev.* **136**, B864-B871 (1964).

[17] Kohn, W. & Sham, L. J. Self-consistent equations including exchange and correlation effects. *Phys. Rev.* **140**, A1133-A1138 (1965).

[18] Oikkonen, L. E., Ganchenkova, M. G., Seitsonen, A. P. & Nieminen, R. M. Vacancies in $CuInSe_2$: new insights from hybrid-functional calculations. *J. Phys.: Condens. Matter* **23**, 422202 (2011).

[19] Oikkonen, L. E., Ganchenkova, M. G., Seitsonen, A. P. & Nieminen, R. M. Redirecting focus in $CuInSe_2$ research towards selenium-related defects. *Phys. Rev. B* **86**, 165115 (2012).

[20] Pohl, J. & Albe, K. Intrinsic point defects in $CuInSe_2$ and $CuGaSe_2$ as seen via screened-exchange hybrid density functional theory. *Phys. Rev. B* **87**, 245203 (2013).

[21] Castleton, C., Höglund, A. & Mirbt, S. Density functional theory calculations of defect energies using supercells. *Model. Simul. Mater. Sci. Eng.* **17** 084003 (2009).

[22] Kresse, G. & Furthmüller, J. Efficiency of ab-initio total energy calculations for metals and semiconductors using a plane- wave basis set. *Comput. Mater. Sci.* **6**, 15 (1996).

[23] Kumagai, Y., Soda, Y., Oba, F., Seko, A. & Tanaka, I. First-principles calculations of the phase diagrams and band gaps in $CuInSe_2$-$CuGaSe_2$ and $CuInSe_2$-$CuAlSe_2$ pseudobinary systems. *Phys. Rev. B* **85**, 033203 (2012).

[24] Perdew, J. P., Burke, K. & Ernzerhof, M. Generalized gradient approximation made simple. *Phys. Rev. Lett.* **77**, 3865-3868 (1996).

[25] Heyd, J., Scuseria, G. E. & Ernzerhof, M. Hybrid functionals based on a screened coulomb potential. *J. Chem. Phys.* **118**, 8207 (2003).

[26] Heyd, J., Scuseria, G. E. & Ernzerhof, M. Erratum: Hybrid functionals based on a screened Coulomb potential [J. Chem. Phys.118, 8207 (2003)]. *J. Chem. Phys.* **124**, 219906 (2006).

[27] Henderson, T. M., Paier, J. & Scuseria, G. E. Accurate treatment of solids with the HSE screened hybrid. *Phys. Status Solidi B* **248**, 4, 767-774 (2011).

[28] Blöchl, P. E. Projector augmented-wave method. *Phys. Rev. B* **50**, 17953 (1994).

[29] Kresse, G. & Joubert, D. From ultrasoft pseudopotentials to the projector augmented-wave method. *Phys. Rev. B* **59**, 1758 (1999).

[30] Bader, R. *Atoms in Molecules: A Quantum Theory* (Oxford University Press, 1990).

Figure captions

Figure 1 (color online). Schematic representation of atomic relaxation (expressed in $\mathring{A}$) of atoms around each vacancy. (a)-(h) denote the relaxations of nearest atoms around the vacant site corresponding to V_{Cu}^{1-}, V_{Zn}^{2-}, V_{S}^{0}, V_{Sn}^{0}, V_{Sn}^{1-}, V_{Sn}^{2-}, V_{Sn}^{3-} and V_{Sn}^{4-}, respectively.

Figure 2 (color online).The local density of states (LDOS) corresponding to the four nearest neighbor atoms around the (a)Cu (b)Zn (c)Sn (d)S vacancy with all the possible charge states in a 64-atom supercell using HSE06 functional. The Fermi level is set at zero energy.

Figure 3 (color online). The band structure of parent CZTS, V_{Cu}^{1-}, V_{Zn}^{2-}, V_{S}^{0}, V_{S}^{2+} and Sn vacancy with 0, 1-, 2-, 3- and 4- five different charge states calculated in a 64-atom supercell within HSE06 functional. The dashed lines illustrate the defect-induced single particle levels within the band gap.

Figure 4 (color online). The local density of states (LDOS) corresponding to the four nearest neighbor atoms around the vacant site for V_{Cu}^{1-}, V_{Zn}^{2-}, V_{Sn}^{0} and V_{Sn}^{1-} in a 432-atom

supercell within PBE functional. The Fermi level is set at zero energy.

Figure 1

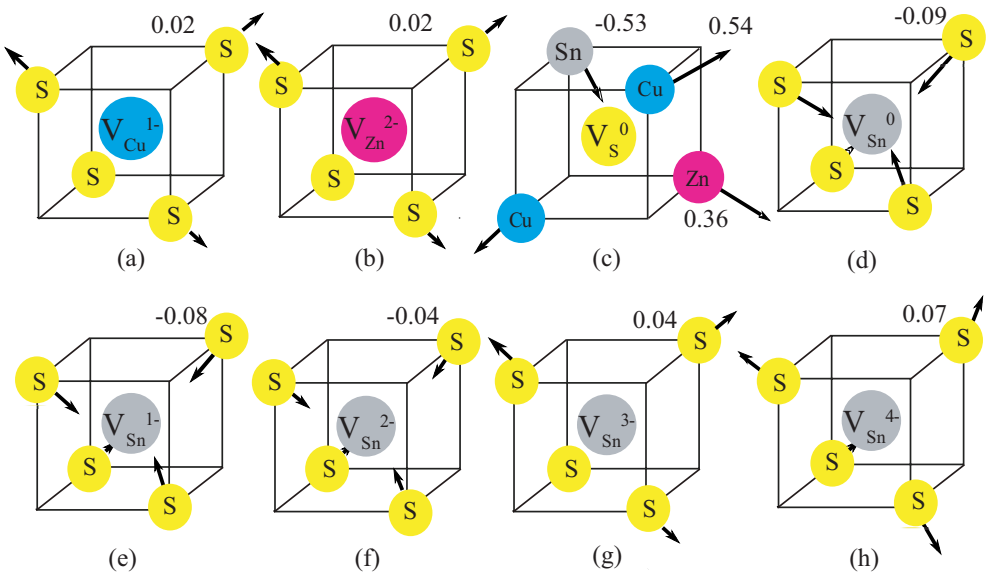

Figure 2

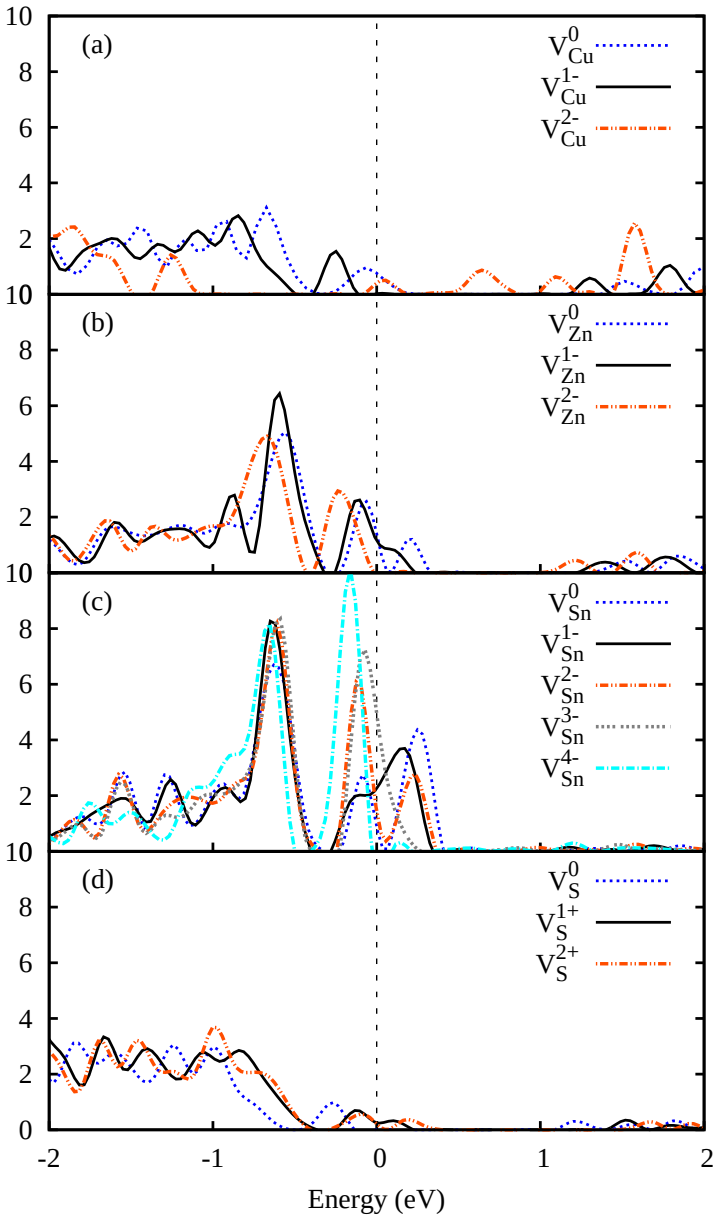

Figure 3

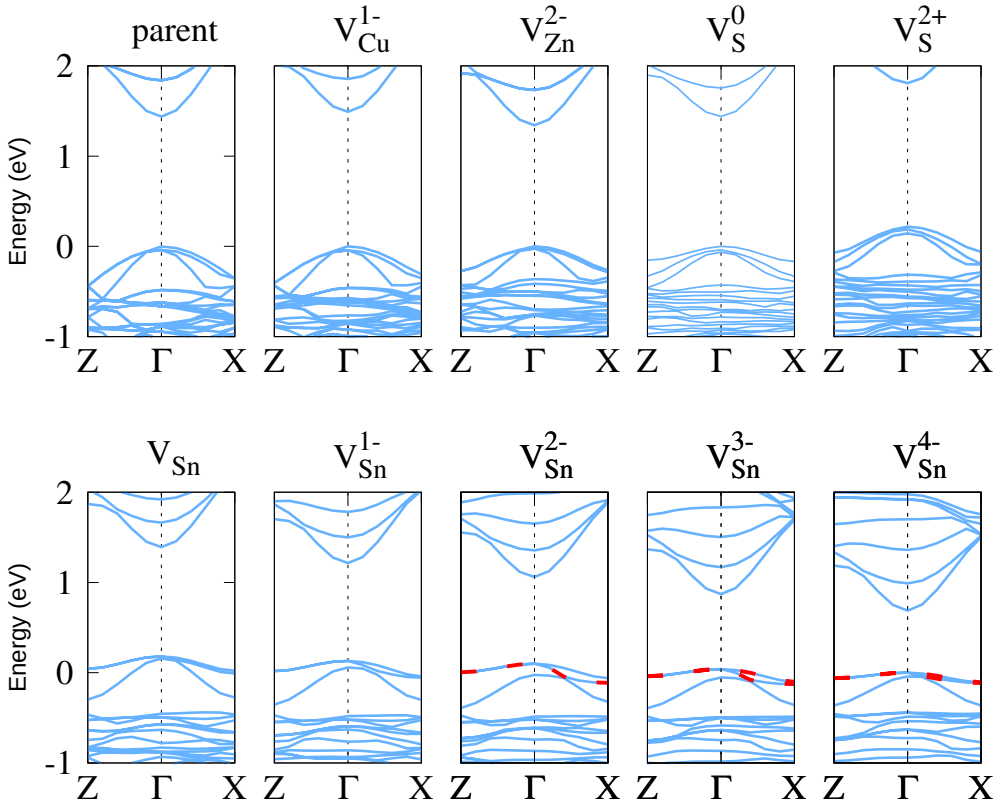

Figure 4

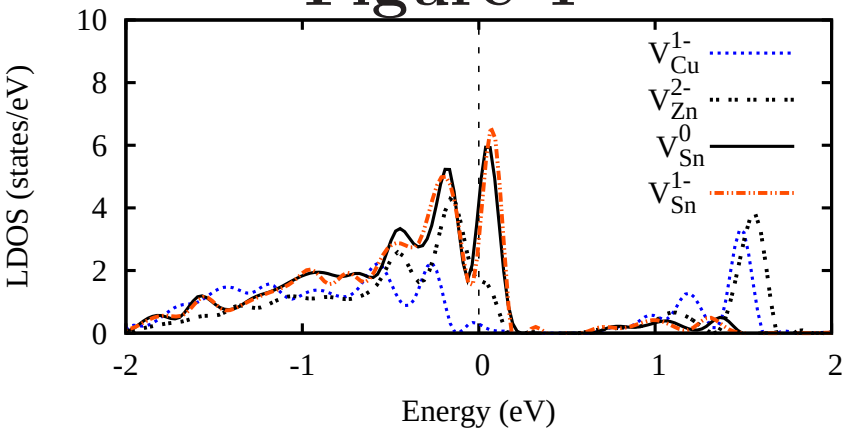

	Cu	Zn	Sn
parent	10.53	11.14	12.62
V_S^0	10.57	11.19	13.11
V_S^{2+}	10.55	11.18	13.08
V_S^0 - parent	0.04	0.05	0.49
V_S^{2+} - V_S^0	-0.02	-0.01	-0.03

Table I. The calculated Bader charge of Cu Zn and Sn atoms around the S vacancy for V_S^0 and V_S^{2+} as well as that of the corresponding atoms for parent CZTS.